FLUCOME 2009
10th International Conference on Fluid Control, Measurements, and Visualization
August 17–21, 2009, Moscow, Russia

PLIF MEASUREMENTS AROUND EVAPORATING MONODISPERSE DROPLET STREAM

Alain Strzelecki[1], Bruno Frackowiak[1,2] and Gerard Lavergne[1]

ABSTRACT

The modelling of the droplet evaporation phenomena in dense sprays is preponderant for a good numerical prediction of the performances of combustion chambers. Empirical correlations derived from basic experiments are often used in numerical codes to take into account the effect of droplet concentration on the dynamical and thermal behaviour of the droplets . A Planar Laser Induced Fluorescence (PLIF) measurement of the vapor mole fraction field is developed around acetone monodisperse droplet streams. The intensity of fluorescence is proportional to the local concentration for given temperature, pressure and laser power. However, the difference of fluorescent signals between the liquid and gas phases induces blooming effect. An interface positioning method based on the Lorenz-Mie Theory (LMT) and on the geometrical optic is proposed on the images with the liquid phase despite the blooming effect. This accurate position is necessary to eliminate the blooming subsequently by hiding the liquid. Experimental results are obtained with two cases of acetone jet injected in a quiescent air at ambient temperature and pressure. They show a good agreement with Flow Simulation except in the close zone of the liquid due to the presence of the mask.

Keywords: PLIF, Fuel evaporation, droplet, blooming

INTRODUCTION

Droplet evaporation modeling in dense sprays is indispensable for providing accurate simulations in a combustion chamber. However, the evaporation phenomenon is complex and hypotheses must be made to ensure reasonable computation times. These hypotheses result from investigations on basic configurations, allowing complete numerical simulations (Abramzon et al, 1989; Dwyer et al, 2000) and experimental measurements (Virepinte et al, 2000; Laurent et al, 2006). Monodisperse droplet streams are commonly used on experimental devices, associated with non-intrusive measurements of the droplet average temperature or diameter: rainbow thermometry, shadowscopy, infrared thermometry and Laser Induced Fluorescence (LIF). Moreover, the wake effect is studied by controlling the distance between two consecutive droplets. Planar Laser Induced Fluorescence (PLIF) is a specific application of the LIF

[1] ONERA , BP 4025-2 avenue E. Belin 31055 Toulouse Cedex 4 France, Corresponding author:e-mail: alain.strzelecki@onera.fr
[2] SLA-Technische Universität Darmstadt, Petersenstrasse 30,D-64287 Darmstadt, Germany

technique providing the 2D vapor fields corresponding to the plane of a thin Laser sheet. Investigations performed on acetone air mixtures and on sprays have highlighted several difficulties inherent to the PLIF technique. Indeed, the high acetone concentration in the liquid phase and the refraction at the interface makes the UV light distribution in the liquid phase non-uniform. Otherwise, the high acetone concentration difference between the liquid and the gas phase leads to a blooming phenomenon. A blooming correction has been proposed according to investigations with Mie scattering images (Orain et al, 2005; Castanet et al, 2007) from non-fluorescing ethanol droplets. Nevertheless, this method implies the use of a specific CCD captor, which in turn requires that the droplet surface position and its vapor mole fraction be precisely known. The droplet surface positioning is consequently delicate. Classical threshold methods result in overestimation of the droplet diameter. Considering the interface as an inflexion point on the extracted fluorescence profiles (Orain et al, 2005) makes physical sense, because the phase change at the interface generates in theory a light intensity step with an infinite derivative. However, the position of the inflexion point is shifted considerably by the blooming, and its determination brings additional numerical uncertainties by derivating a sampled profile. Another strategy relies on methanol droplets seeded with acetone and injected with the same experimental parameters as the acetone droplets (Bazille et al, 1994). The resulting liquid fluoresces slightly without the incident signal absorption, as methanol is transparent under UV light. The droplet surface is easily determined on the images, and this positioning is assumed to be the same for the images of the acetone droplets. However, the differences in the methanol physical properties and a high sensitivity of the jet to the experimental parameters affect the droplets size and the jet direction, increasing the uncertainties in this positioning. The objective of this work is to achieve a precise 61 interface positioning strategy on the images with the liquid phase and to eliminate the blooming elimination subsequently. A method based on the Lorenz-Mie Theory (LMT) (Castanet et al, 2005; Mees et al, 2001) and on the geometrical optic is proposed to model the liquid phase fluorescence and to locate the interface regarding the fluorescence maximum, despite the blooming effect. The blooming is eliminated by performing two consecutive measurements on the same configuration of a monodisperse acetone droplet stream, first with a mask hiding the liquid phase, and then without. In the first case, the fluorescence signal is not affected by the blooming, whereas in the second case the interface is successfully positioned. A quantitative vapor mole fraction profile is obtained from the fluorescence images in the droplet equatorial plane; comparison with the numerical simulations validates the method. Moreover, the numerical simulations provide the temperature fields around the droplet, leading to a precise analysis of the influence of this parameter.

FLUORESCENCE THEORY AND SIMPLIFYING HYPOTHESES

The fluorescence is a radiative de-excitation process affecting the acetone molecules illuminated by an incident monochromatic Laser light at a specific excitation wavelength. The fluorescence signal S_{fluo}, expressed as a number of photons, is linked to the local acetone mole fraction $X_{acetone}$ (1), by considering the quantum yield $\Phi(\lambda_{laser}, P, T))$ and the absorption cross section $\sigma(\lambda_{laser}, T)$.

$$S_{fluo} = \frac{E}{hc/\lambda_{laser}} . \eta_{optic} . dV_c . \left[\frac{X_{acetone} . P . N_A}{R . T} \right] . \sigma(\lambda_{laser}, T) . \Phi(\lambda_{laser}, P, T) \quad (1)$$

The Laser wavelength, the optical collection efficiency, and the collection volume are determined with the experimental device, whereas the Laser fluence, temperature, pressure and vapor mole fraction are local parameters in the investigated vapor field. According to previous work (Thurber et al, 1998) the quantum yield dependence on the local pressure is negligible under 5 bars. Otherwise, the fluorescence dependence on the local temperature relies on the quantum mechanics to model the absorption cross section $\sigma(\lambda_{laser}, T)$ and the fluorescence quantum $\Phi(\lambda_{laser}, P, T))$. Interpolation of Thurber results

[16] led to a polynomial correction $f_1(T)$ (2) for temperatures ranging from 20°C to 700°C , assuming the pressure to be fixed at a reference value P_{ref} , and for a given wavelength λ_{laser} .

$$f_1(T) = \frac{\Phi(\lambda_{laser}, P_{ref}, T).\sigma(\lambda_{laser}, T).T_{ref}}{\Phi(\lambda_{laser}, P_{ref}, T_{ref}).\sigma(\lambda_{laser}, T_{ref}).T} \qquad (2)$$

Other phenomena affect the fluorescence quantitative measurement. Quenching is a non-radiative relaxation process resulting from the collision between the acetone and other molecules such as oxygen molecules. This phenomenon is indirectly taken into account in the polynomial correction $f_1(T)$ (2). The phosphorescence corresponds to a secondary radiative de-excitation process to lower energy quantum states that is difficult to model. Nevertheless, its characteristic time is longer compared with the fluorescence time. Moreover, the influence of quenching on the phosphorescence is significant, strongly limiting this radiative process. In the confined test rigs, photolysis occurs, resulting in the dissociation of the acetone molecules. The available excitation energy as well as the acetone mole fraction are consequently reduced, limiting the fluorescence. According to Thurber results (Thurber, 1999), the photo-dissociation affects 10% of the acetone molecules after 1000 Laser shots, for a Laser fluence averaging 1000 mJ.cm $^{-2.}$

EXPERIMENTAL SETUP

The experimental device (Fig. 1) is based on the acquisition of fluorescence images corresponding to a thin UV Laser sheet which interacts with the acetone molecules, either in a saturated hermetic cell for the calibration, or with the monodisperse droplets stream. A 266 nm 10 Hz pulsed ND-YAG Laser beam is transformed into a thin parabolic sheet through an adjustable optical device. The minimum size and thickness of the sheet average 50 mm and 300 µm respectively, at a position which matches the experimental area. The Laser energy is set by orientating the polarization wave plate at the entrance of the harmonic generator.

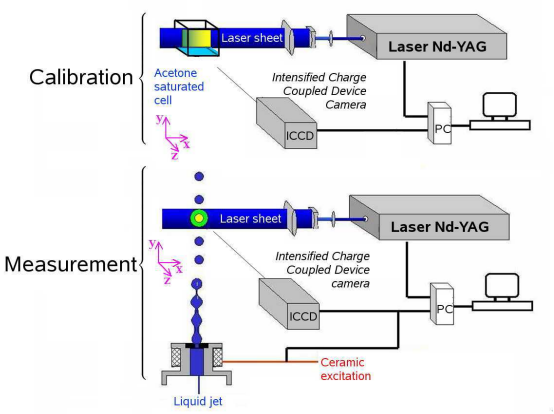

Fig. 1 Experimental test rig

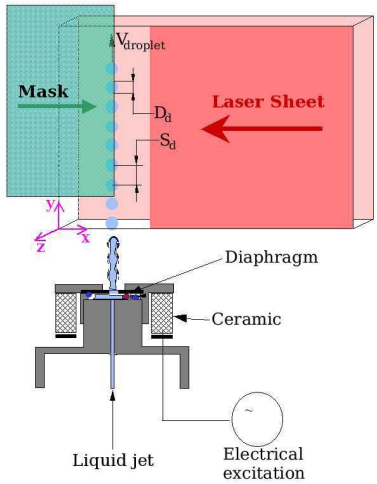

Fig. 2 Monodisperse droplet jet and mask positioning

The excited acetone molecules fluoresce in the visible wavelength, ranging from 350 to 550 nm. A band pass optical filter corresponding to this wavelength interval is used on the lenses, eliminating the scattered UV light. In addition, the field depth of the camera is superior to the sheet thickness, through the use of an aperture of 5.6. The camera associated with the phosphorus intensifier and the post processing software acquires instantaneous images each corresponding to the fluorescence field averaged on the sheet thickness. The image resolution is 13 µm/pixel, and the camera has a dynamic range of 12 bits. The signal noise is reduced by averaging 100 instantaneous images before post processing. A semi-transparent mirror takes 20 % of the Laser beam for the measuring device. Therefore, the measured value E_{laser} corresponds to 25 % of the Laser energy affecting the experiment during 1 pulse. The average value of the background noise is measured in the ambient air at some distance from the jet or outside the cell on the same image, where the acetone mole fraction is negligible. All the images shown rely on the same Cartesian reference mark (Fig. 1): x corresponding to the Laser sheet opposite direction, y corresponding to the monodisperse droplet stream direction, from the bottom to the top, and z orthogonal to the Laser sheet plane, towards the camera.

The calibration with a hermetic cell

A calibration is performed by measuring the fluorescence 1D-profile in the Laser sheet direction (x coordinate) from a saturated acetone hermetic cell (Fig. 1). The general fluorescence equation (1) is adapted to the experimental device , considering the measured relative value $\frac{S_{fluo}}{S_{ref}}$ obtained with the acquisition device. The local Laser fluence E is rewritten as a function of the Laser fluence outside the cell E_∞, also taking into account the absorption in the cell between the window position x_{window} and the considered position x, as the transmission factor T_{cell} through the cell windows. Moreover, the pressure and the temperature are uniform and equal to their respective ambient values P_0 and T_0.
The vapor mole fraction in the cell is consequently uniform, and calculated with the Antoine correlation . This results in an exponential fluorescence 1D-profile in the Laser sheet direction (x) which is fitted to the measured overlapping profiles with a least-squares method (Fig. 2). The Laser fluence outside the cell E_∞ depends only on the measured Laser energy. Several Laser fluence values outside the cell have been calculated from fluorescence 1D-profiles obtained under the same ambient pressure and temperature at different measured Laser energy E_{laser} .

Measurement around the monodisperse droplet stream

The monodisperse droplet stream (Fig. 3) is based on the Rayleigh disintegration of the liquid jet through a piezo ceramic, providing calibrated droplets with the same size, the same velocity, the same temperature and the same spacing parameter $C = \frac{S_d}{D_d}$ at a given distance from the injector. Therefore, measurements at different positions result in a temporal evolution of a considered droplet in the jet. The spacing parameter is set to comply with the frequency of the ceramic and the velocity with the pressure at the injector tank. The mass flow rate conservation yields the droplet diameter at the injector (3), and its decrease in the stream resulting from the evaporation is ignored.

$$D_d = \sqrt[3]{\frac{3.\Phi_0^2.S_d}{2}} \quad (3)$$

The injection temperature is regulated with the thermostat. Moreover, fine screws adjust the liquid

jet orientation so that the droplets are entirely illuminated by the Laser sheet. A mask positioned in front of the droplets by micrometric screws can hide the liquid phase and eliminate the blooming effect in the vapor phase. The camera, the ceramic frequency and the Laser pulses are synchronized in order to get fixed droplets on each instantaneous image. A shadowscopy device made up of a CCD visible camera, a macro- scopic lens and a monitor synchronized on the droplet injector controls the stability of the stream.
The advantage of the PLIF technique concerns the vapor phase surrounding the droplets, on the side towards the Laser. In a first approach, the local temperature variations in the vapor phase are ignored and only the ambient value T_1 is considered. This hypothesis will be validated by the numerical model description at the end of the paper. The local pressure variation is also ignored and only the ambient value P_1 is considered. The previous fluorescence equations used for the calibration are adapted to this configuration without the hermetic cell, by ignoring the absorption in the gas phase. The Laser fluence is consequently uniform, and corresponds to the function $\boldsymbol{E_\infty}$ determined at the calibration. The cell window transmission factor $\boldsymbol{T_{cell}}$ disappears, whereas the ambient temperature and pressure influence are taken into account through the respective ratios $\frac{\boldsymbol{f_1(T_1)}}{\boldsymbol{f_1(T_0)}}$ and $\frac{\boldsymbol{P_1}}{\boldsymbol{P_0}}$.

$$\frac{\boldsymbol{S_{fluo}}}{\boldsymbol{S_{ref}}} = \boldsymbol{K(T_0, P_0)}.\frac{\boldsymbol{f_1(T_1)}}{\boldsymbol{f_1(T_0)}}.\frac{\boldsymbol{P_1}}{\boldsymbol{P_0}}.\boldsymbol{E_\infty}.\boldsymbol{X_{acetone}} \quad (4)$$

For a chosen experimental configuration, several acquisitions are performed, with the mask moved progressively, to hide the liquid phase increasingly, in order to keep most of the vapor phase fluorescence and to hide all the droplets. The mask must be at a sufficient distance from the droplets to avoid the aerodynamic interactions, and remain close to the field depth of the camera to limit the blurring effect on the images. Due to this position outside the field depth of the camera, residual light from the liquid phase would affect the fluorescence if the mask edge corresponded exactly to the surface of the droplets. A part of the vapor phase is consequently hidden. The postprocessed images with the droplet surface vapor mole fraction as threshold highlight the significant effect of the blooming. Without the mask, the interface position is wrong. With a partially hidden liquid phase, residual light coming from the liquid phase depicts the shape of the droplets and leads overestimation of the vapor mole fraction. The droplet surfaces are therefore positioned precisely on the images without the mask, despite the overestimation of the fluorescence. The mask is afterwards delicately moved without modifying the droplet stream, making the interface position identical on the images. Regarding the quantitative analysis of the acetone mole fraction in the gas phase, the advantage concerns the 1D profiles extracted from the fluorescence images , corresponding to the equatorial plane of the droplets.

LIQUID PHASE FLUORESCENCE MODELING AND INTERFACE POSITIONING

The proposed interface positioning relies on the fluorescence modeling according to both the Lorenz-Mie Theory (LMT) for the incident Laser fluence $\boldsymbol{E_{liq}}$ inside the droplet and to the geometrical optic for the fluorescence rays generating the 1D profile.

Computation of the UV Laser fluence field

The UV Laser fluence field $\boldsymbol{E_{liq}}$ (Fig. 7) is computed in the liquid phase with a code based on the LMT [9,21]. The model is based on the complete resolution of the Maxwell equations inside a sphere

illuminated by a continuous monochromatic plane wave at 266 nm . The computation is axisymmetric, and the refractive index inside the sphere is uniform. The droplet equatorial plane generated by the x and z axes is considered. . The absorption is taken into account through the imaginary part of the complex refractive index. The light scattering is also modeled.

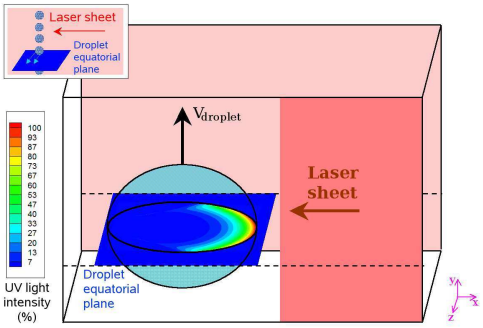

Fig. 3 Incident Laser fluence in a 200 µm droplet obtained with the code based on the LMT

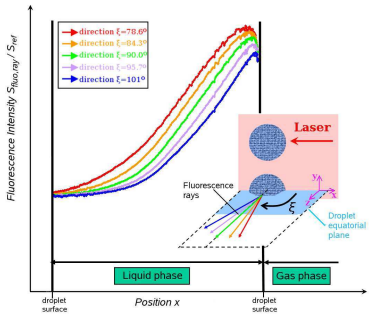

Fig. 4 Computed fluorescence profiles corresponding to the liquid phase for different directions ξ

The computed UV Laser fluence field highlights that light absorption in the liquid phase is a dominant factor, with the maximum incident light located at the surface on the side towards the Laser. An exponential decrease inside the droplet is observed. The first order refraction rays at the droplet surface tend to bend the iso-intensity layers towards the droplet centre.

Computation of intensity of the fluorescence rays

The rays generating the fluorescence profile are included in the camera angular field, which averages 10°. In a first approximation, the rays emerging from the droplet surface and orthogonal to the laser sheet are analyzed (Fig. 8) and these directions correspond to the z axis. These rays emerge from the droplet equatorial circle. Basic geometry considerations provide the angle θ of these rays with the normal direction to the droplet surface. The Snell-Descartes law combined with the optical reciprocity principle gives the direction of the rays in the liquid phase.

$$S_{fluo,liq} = \frac{E_{liq}}{hc/\lambda_{laser}}.\eta_{optic}.dV_c.\left[\frac{\rho_{liq}.N_A}{M}\right].\sigma(\lambda_{laser},T_{liq}).\Phi(\lambda_{laser},P_{liq},T_{liq}) \qquad (7)$$

Assuming the temperature, pressure and density to be uniform and the fluorescence to be isotropic in the liquid phase, the signal $S_{fluo,liq}$ is proportional to the local UV Laser fluence E_{liq}, with the same factor at every point in the droplet (8). In contrast to the UV incident light at 266 nm, the fluorescence signal is not absorbed by the acetone in the wavelength range (350-550 nm). The fluorescence contribution of a ray is deduced by adding the fluence values on each discrete volume of the liquid phase intersecting the ray (8), taking into account the transmission fact or $T_{dioptre}$ over all the droplet surface.

$$S_{fluo,ray} = T_{dioptre}.K_l(T_{liq},P_{liq}).\int_{ray} E_{liq}.dV_C \qquad (8)$$

Fluorescence image corresponding to the liquid phase

The fluorescence contribution of each discrete emerging ray is consequently computed knowing the incident UV light field inside the droplet. Plotting these contributions versus the x cartesian coordinates provides the fluorescence profile generated by the orthogonal to the Laser sheet rays $(\xi = 90°)$. However the real fluorescence profile is generated by the emerging rays whose direction _ is included in the camera angular field. A further refinement consists in performing the same computation for the rays included in the droplet equatorial plane (generated by the x and z axes), with a different direction ξ than the orthogonal rays. In each computation, the direction with the Laser sheet plane ξ is fixed for all the emerging rays at the droplet surface. The fluorescence contributions $\frac{S_{fluo,ray}}{S_{ref}}$ are plotted against the x Cartesian coordinates for each given direction ξ (Fig. 4).For the angles ξ included in the camera field, the resulting profiles (Fig. 4) present a maximum located close to the droplet surface, at a distance equal to 5 % of the radius. The simulated fluorescence profile corresponding to the droplet equatorial plane is an average of all these profiles and the distance between its maximum and the droplet surface is also equal to 5 % of the radius. The simulated fluorescence profile corresponding to the droplet equatorial plane is an average of all these profiles and the distance between its maximum and the droplet surface is also equal to 5 % of the
radius.

RESULTS AND DISCUSSION

The parametrical study with droplets injected in the ambient air (Table 1.) focuses on the influence of the injection temperature, droplet diameter and spacing parameter $C = \frac{S_d}{D_d}$ on the concentration of the vapor. The diaphragm diameter is fixed at 100 μm.

Table 1. Experimental parameters

Profile	Injection temperature	Droplets diameter	Parameter $C = \frac{S_d}{D_d}$	Droplets velocity	Frequency
a	21.6 °C	265 μm	4.67	8.19 m.s-1	6617 Hz
b	22.4°C	173 μm	2.00	7.87 m.s-1	22687 Hz
c	45.6°C	238 μm	3.76	8.30 m.s-1	9287 Hz
d	45.5°C	181 μm	2.20	7.15 m.s-1	17987 Hz
e	45.6°C	169 μm	1.92	8.59 m.s-1	26497 Hz

Interface positioning and blooming effect

A first qualitative analysis is carried out with droplets injected at 45.6 °C. All the profiles presented, with or without the mask, are extracted from different droplets on the same image (Fig. 5, Fig. 6). The profiles extracted from the images without the mask (Fig. 5) show a sharp maximum on the side towards the laser, whereas the decrease is moderate on the opposite side. The interface is easily positioned from the maximum, according to the liquid phase fluorescence model, since the droplet diameter is known. Indeed, the maximum position of the experimental profiles is not affected by the blooming, and the proposed interface positioning can be applied on the bloomed images. This method leads to a point closer to the maximum, compared with the classical positioning on the inflexion point (Orain et al, 2005). The

difference $\Delta s / D_d$ (Fig. 5) ranges between 10 % and 16 % of the droplet diameter (Table 2). It results both from the inflexion point calculation with the sampled values and from the blooming effect which shifts this inflexion point.

Table 2. Difference between the proposed interface positioning and the classical positioning on the inflexion point

Profile	Droplet diameter	Difference $\Delta s / D_d$ in the interface position
a	265 µm	10%
b	173 µm	15%
c	238 µm	12%
d	181 µm	16%
e	169 µm	15%

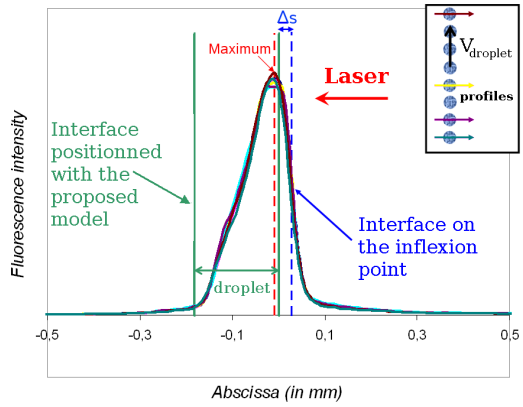

Fig. 5 Interface positions on the extracted fluorescence profiles (corresponding to the equatorial planes of different droplets)

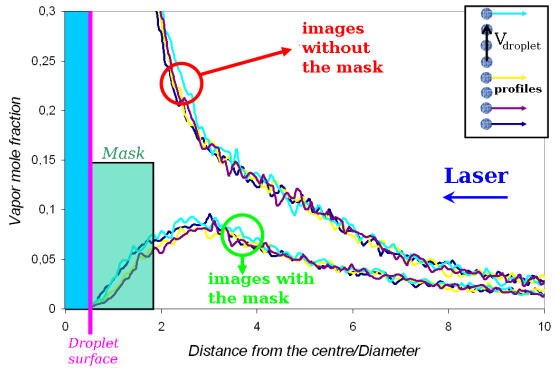

Fig. 6 Influence of the mask on the fluorescence profiles (corresponding to the equatorial planes of different droplets)

The comparison between the profiles corresponding to the images with and without the mask (Fig. 6) highlights the strong effect of the blooming affecting the fluorescence signal in a large part of the vapor field (at a distance bordering on 10 droplet diameters). The profiles obtained with the mask represent the vapor mole fraction only on their decreasing part. All the quantitative profiles are similar and included in the uncertainty margin, highlighting the weak evolution of the vapor mole fraction on the camera field. Therefore, only one profile is retained for each configuration. The increasing part of the profiles results from a slight contribution of the points behind the mask on the fluorescence image, the mask being positioned outside the field depth of the camera.

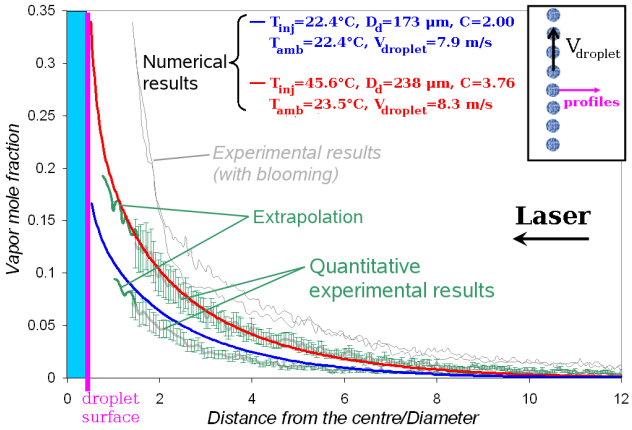

Fig. 7 Acetone vapor mole fraction profiles. Comparison between the numerical and experimental results

Fig.7 compares experimental acetone mole fraction profiles obtained with numerical simulation. The numerical simulation consists to couple Navier Stokes equations computation inside the droplet with external flow calculations. In the case of the stream, axisymmetry is assumed and computation is 2D. Unsteady coupling is performed between the two codes to insure the boundary conditions at the droplet surface including Marangoni effect. The external flow of the stream is modelled with two consecutives half droplets and a periodic condition between the inlet and the outlet of the domain is set. The monodisperse jet is considered therefore as infinite. Experimental results (Fig. 7) are obtained with two cases of acetone jet injected in a quiescent air at ambient temperature and pressure. They show a good agreement with the numerical model except in the close zone of the liquid due to the presence of the mask.

CONCLUSION

The PLIF measurement technique has been successfully developed around the monodisperse droplet stream, for different injection temperatures, spacing parameters and droplet diameters. Relevant results in agreement with the numerical simulations have been obtained. A simplified liquid phase fluorescence modeling based on the LMT and on the geometrical optic yielded an interface positioning method applicable to the fluorescence images affected by the blooming phenomenon. This accurate interface position allowed the effects of blooming to be counteracted, by hiding the liquid with a mask without modifying the parameters. Such a positioning method is necessary to apply the blooming correction based on the Mie scattering images with the appropriate CCD captor. The correct agreement between the numerical and experimental results helps to validate the numerical model, which is extended to more complex configurations, in order to refine the existing correlations applied in the combustion chamber simulations..

ACKNOWLEDGMENTS

This work has been supported by the French environment agency (ADEME) and the car manufacturer Renault for its contribution to improve combustion in engines and reduce the pollutant emissions.

REFERENCES

Abramzon B., Sirignano W. A. (1989) Droplet vaporization model for spray combustion calculations. Int. J. Heat and Mass Transfer 32: 1605-1618

Niazmand H., Shaw B. D., Dwyer H. A., Aharon I. (1994) Effects of Marangoni convection on transient droplet evaporation. Combustion Science & Technology 103: 219-233

Dwyer H. A., Stapf P., Maly R. (2000) Unsteady vaporization and ignition of a three-dimensional droplet array. Combustion and Flame 121: 181-194

Virepinte J.F., Magre P., Collin G., Lavergne G., Biscos Y. (2000) A rectilinear droplet stream in combustion: droplet and gas phase properties. Combustion Science & Technology 150: 143-159

Castanet G., Lavieille P., Lemoine F., Lebouch´e M., Atthasit A., Biscos Y.,

Lavergne G. (2002) Energetic budget on an evaporating monodisperse droplet stream using combined optical methods. Evaluation of the convective heat transfer. Int. J. Heat and Mass Transfer 45: 5053-5067

Atthasit A., Doue N., Biscos Y., Lavergne G. (2003) Influence of droplet concentration on the dynamics and evaporation of a monodisperse stream of droplets in evaporation regime. In: 1st 472 International symposium on combustion and atmospheric pollution, St Petersburg, Russia

Frackowiak B., Lavergne G., Grehan G., Mees L. (2004) 474 Improvement of the rainbow technique for thermal gradient evaluation inside a droplet. In: 7th 475 Int.Congress on Optical Particle Characterization, Kyoto, Japan

Lavieille P., Delconte A., Blondel D., Lebouch´e M., Lemoine F. (2004) Non intrusive temperature measurements using two-color-Laser-induced fluorescence. Experiments in Fluids 36: 706-716

Castanet G., Delconte A., Lemoine F., Mees L., Grehan G. (2005) Evaluation of temperature gradients within combusting droplets in linear stream using two colors Laser Induced Fluorescence. Experiments in Fluids 39: 431-440

Saengkaew S., Charinpanitkul T., Mees L., Grehan G. (2006) Rainbow refractometry: on the validity domain of Airy's and Nussenzweig's theories. Opt. Commun. 259: 7-13

Laurent C., Biscos Y., Doue N., Maqua C., Lemoine F., Grehan G., Lavergne G. (2006) Thermal gradient determination inside vaporizing droplet by combining rainbow and Laser Induced Fluorescence measurements. In: European Fluids Engineering Summer meeting, Miami, USA

Ritchie B. D., Seitzman J. M. (2001) Quantitative acetone PLIF in two-phase flows. AIAA 2001-0414

Grisch F., Bresson A., Bouchardy P., Attal-Tretout B. (2002) Advanced optical diagnostic applied to dynamic flames and turbulent jets. Aerospace Science and Tech. 6: 465-479

Ritchie B. D., Seitzman J. M. (2004)Simultaneous Imaging of Vapor and Liquid Spray Concentration Using Combined Acetone Fluorescence and Phosphorescence. AIAA 2004-0384

Orain M., Mercier X., Grisch F. (2005) PLIF imaging 498 of fuel-vapor spatial distribution around a monodisperse stream of acetone droplets: comparison with modelling. Combustion Science & Tech. 177: 249-278

Thurber M. C. (1999) Acetone Laser Induced Fluorescence for temperature and multiparameter imaging in gaseous flows. Thesis report TSD-120, Stanford University

Thurber M. C., Grisch F., Kirby B. J., Vostmeier M., Hansom R. K. (1998), Measurements and modelling of acetone Laser Induced Fluorescence with implication for temperature imaging diagnostics. Applied Optics 37: 4963

Yuen L. S., Peters J. E., Lucht R. P. (1997) Pressure dependence of Laser Induced Fluorescence from acetone. Applied Optics 36: 3271

Castanet G., Maqua C., Orain M., Grisch F., Lemoine F. (2007) Investigation of heat and mass transfer between the two phases of an evaporating droplet stream using Laser-induced fluorescence techniques: Comparison with modeling. International Journal of Heat and Mass Transfer 50: 3670-3683

Bazile R., Stepowski D. (1994) Measurements of the vaporization dynamics in the development zone of a burning spray by planar Laser induced fluorescence and Raman scattering. Exp. In Fluids 16: 171-180

Mees L., Gouesbet G., Gr´ehan G. (2001) Interaction between femtosecond pulses and a spherical microcavity: internal fields. Optics Communications 199: 33-38

Ossler F., Alden M. (1997) Measurements of picosecond Laser Induced Fluorescence from gas 3-pentanone and acetone: implications in combustion diagnostics.Applied Physics B 64: 493-502

Grossmann F., Monkhouse P. B., Ridder M., Sick V., 522 Wolfrum J. (1996) Temperature and pressure dependences of Laser Induced Fluorescence of gas phase acetone and 3-pentamone. Applied Physics B 62: 249-253

Van Cruyningen I., Lozano A., Hanson R. K. (1990) Quantitative imaging of concentration by Planar Induced Fluorescence. Exp. In Fluids 10: 41-49

Schulz C., Sick V. (2005) Tracer-LIF diagnostics: Quantitative measurement of fuel concentration, temperature and air/fuel ratio in practical combustion situations. Prog. Energy Combust. Sci. 31: 75-121

National Institute of Standards and Technology (NIST) Chemistry WebBook, http://webbook.nist.gov (2005)

Frackowiak B., Strzelecki A., Lavergne G. (2006) Tridimensional computation of interactions between evaporating droplets. In: 31st 533 International Symposium on Combustion, Heidelberg, Germany

Frackowiak B., Strzelecki A., Lavergne G. (2007) Vapor concentration measurement around vaporizing droplets by the PLIF technique. Comparison with the numerical simulation. In: 6th 537 International Conference on Multiphase Flow, ICMF 2007, Leipzig, Germany

Fluent Inc. Copyright, http://www.fluent.com

RanzW. E., MarshallW. R. (1952) Evaporation from drops. Chem. Eng. Progr.48: 141-146, 173-180